

Neural Encoding and Decoding with Deep Learning for Dynamic Natural Vision

Haiguang Wen^{2,3†}, Junxing Shi^{2,3†}, Yizhen Zhang^{2,3}, Kun-Han Lu^{2,3}, Zhongming Liu^{*1,2,3}

How does the brain represent visual information from the outside world? Here, we approach this question with a deep convolutional neural network that mimics neuronal circuitry and coding, and learns to solve computer vision tasks. Using this network as a computational model of the visual cortex, we develop novel encoding and decoding models to describe the bi-directional relationships between visual input and cortical activity measured with functional magnetic resonance imaging. Testing these models with imaging data from humans watching natural movies, we show that the encoding model can predict cortical responses and retrieve visual representations at individual brain locations, and that the decoding model can decipher the measured cortical activity to reconstruct the visual and semantic experiences. Both the encoding and decoding models utilize cortical representations of hierarchical, invariant, and nonlinear visual features. Being self-contained, efficient, and generalizable, these models constitute a computational workbench for high-throughput investigation of all stages of visual processing. We also anticipate that the general strategy for neural encoding and decoding via deep-learning models will be applicable to other sensory or cognitive experiences, e.g. speech, imagery, memories and dreams.

Neural encoding | brain decoding | deep learning | natural vision

Significance Statement: this study brings major advances in encoding and decoding cortical activity that supports human natural vision. For encoding, we demonstrate the unique promise of using deep learning to model and visualize the functional representations at the level of single cortical locations along the entire visual pathway, and to create a computational workbench for high-throughput vision research. For decoding, we present a stand-alone, efficient, reliable, and generalizable strategy to decode cortical fMRI activity to directly reconstruct the visual and semantic experiences during natural vision. These unique capabilities highlight a promising emerging direction of using the artificial brain to understand the biological brain.

Introduction

For centuries philosophers and scientists have tried to speculate, observe, understand, and eventually decode

the workings of the brain that enables the human natural vision. The central questions are how the brain represents visual information from the outside world, and whether one may decode brain activity to reconstruct what a person is seeing. These questions, generally known as neural encoding and decoding, have been mostly approached with overly simplified strategies that use artificial patterns or static pictures as visual stimuli. However, it remains largely unknown how dynamic and realistic visual experiences are represented along the entire visual pathway. What is needed is an alternative strategy that embraces the complexity of vision to fully uncover and decode the visual representations of distributed cortical activity.

Despite its diversity and complexity, the visual world is composed of a finite number of hierarchical and invariant visual features (Zeiler and Fergus, 2014; LeCun et al., 2015; Russ and Leopold, 2015), including those in the low-level visual space (e.g. orientation and color), the middle levels (e.g. shape and texture), and the high-level semantic space (e.g. face and house). In the brain, these features emerge from cascaded stages of visual processing (Felleman and Van Essen, 1991; Dicarlo et al., 2012; Russakovsky et al., 2015) via complex neural circuits. To decipher natural vision, a more effective strategy is to identify and decode neural representations of visual features at all levels, rather than attempting to relate brain activity to infinite pixel combinations. In this regard, we model neural representations using visual features extracted by brain-inspired deep learning (LeCun et al., 2015): a class of deep artificial neural networks trained to emulate or surpass human performance in computer-vision tasks (Russakovsky et al., 2015). Recent studies also show that such network models are well aligned to and predictive of cascaded cortical processes underlying visual perception (Khaligh-Razavi and Kriegeskorte, 2014; Yamins et al., 2014; Güçlü and van Gerven, 2015a,b; Cichy et al., 2016). In addition, the model is fully observable and computable both forward and backward (Zeiler and Fergus, 2014), such that the extracted features can be transformed, either top-down or bottom-up, to visualize their internal representations, to reconstruct the visual input, as well as to deduce its semantic categorization.

[†] Haiguang Wen and Junxing Shi contributed equally to the work. *Correspondence: zmliu@purdue.edu

¹Weldon School of Biomedical Engineering, ²School of Electrical and Computer Engineering, ³Purdue Institute for Integrative Neuroscience, Purdue University, West Lafayette, Indiana, 47906, USA.

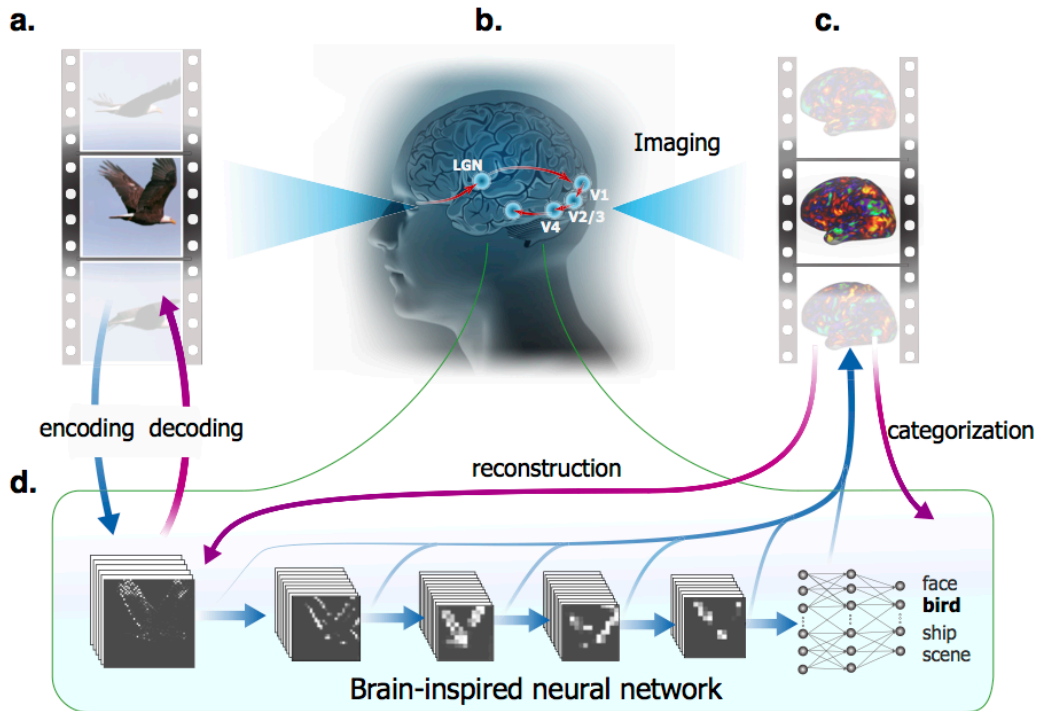


Figure 1. Neural encoding and decoding through a deep learning model. When a person is seeing a film (a), information is processed through a cascade of cortical areas (b), generating fMRI activity patterns (c). A deep convolutional neural network is used here to model cortical visual processing (d). This model transforms every movie frame into multiple layers of features, ranging from orientations and colors in the visual space (the 1st layer) to object categories in the semantic space (the 8th layer). For encoding, this network serves to model the nonlinear relationship between the movie stimuli and the response at each cortical location. For decoding, cortical responses are combined across locations to estimate the feature outputs from the 1st and 8th layer. The former is deconvolved to reconstruct every movie frame, while the latter outputs the semantic descriptions.

Here, we explore this new strategy for encoding and decoding natural vision. We acquired functional magnetic resonance imaging (fMRI) data from three healthy subjects watching natural movies with their eyes fixated at the screen center. The stimuli included two different sets of video clips: one for training the encoding and decoding models, and the other for testing them. Our goals were 1) to develop the encoding model to predict fMRI responses and retrieve visual representations at individual cortical locations, and 2) to develop the decoding model to reconstruct the visual and semantic experiences based on fMRI activity. Towards these goals, we used a deep convolutional neural network (CNN) (Krizhevsky et al., 2012) as a fully accessible model of the human visual cortex. For encoding, the CNN-extracted visual features were projected onto cortical activity; for decoding, cortical activity was converted to image and semantic feature representations. Fig. 1 illustrates our encoding and decoding strategy.

Materials and Methods

Experiments. Three healthy volunteers (female, age: 22-25) watched natural color video clips ($20.3^\circ \times 20.3^\circ$) with a central fixation cross ($0.8^\circ \times 0.8^\circ$). All subjects

were healthy volunteers with normal vision. Informed written consent was obtained from every subject according to the research protocol approved by the Institutional Review Board at Purdue University. In total 276 video clips were included in a 2.4-hour training movie, randomly split into 18 8-min segments; 38 different video clips were included in an 8-min testing movie. Each subject watched the training movie twice and the testing movie ten times with their eyes fixated to a central cross. Experiments were done during several days in ~2 weeks; each day included multiple sessions; in each session, an 8-min movie segment was presented as the visual stimulation. The order of the movie segments was random and counter-balanced across subjects.

Visual stimuli were delivered through a goggle system (NordicNeuroLab NNL Visual System). The display resolution was 800×600 . The stimulus presentation was controlled by using Psychophysics Toolbox 3 (<http://psycho toolbox.org>). The movies were displayed on a black background and scaled to 600×600 pixel arrays.

Data Acquisition and Preprocessing. T_1 and T_2 -weighted MRI and fMRI data were acquired in a 3 tesla MRI system (Signa HDx, General Electric, Milwaukee) with a 16-channel receive-only phase-array surface coil (NOVA Medical, Wilmington). The fMRI data were acquired at 3.5-mm isotropic spatial resolution and 2-s temporal resolution by using a single-shot, gradient-recalled echo-planar imaging sequence (38 interleaved axial slices with 3.5 mm thickness and 3.5×3.5 mm² in-plane resolution, TR/TE=2000/35ms, flip angle=78°, field of view=22×22 cm²). All fMRI images were co-registered, preprocessed, and transformed onto the cortical surfaces by using the processing pipeline developed for the Human Connectome Project, as described in (Glasser et al., 2013). When training and testing the encoding and decoding models (as described later), the cortical fMRI signals were averaged over multiple repetitions of the same movie segment: two repetitions for the training movie and 10 repetitions for the testing movie.

Convolutional Neural Network (CNN). We used a deep CNN (also known as the AlexNet) as a model of the visual cortex to extract hierarchical visual features from the movie stimuli. This model has been pre-trained to achieve the best-performing object recognition in Large Scale Visual Recognition Challenge 2012 (Krizhevsky et al., 2012). This CNN includes eight layers of artificial neurons stacked into a hierarchical architecture: the first five are convolutional layers, and the last three layers are fully connected for object classification. In each convolutional layer, artificial neurons encode a number of features, each of which represents a kernel convolved over its inputs. Layer 1 through 5 consists of 96, 256, 384, 384, and 256 kernels, respectively. Each convolutional layer is composed of some or all of the following four stages: linear filtering, non-linear transformation, max-pooling, and divisive normalization. For classification, layer 6 and 7 are fully connected networks with a rectified linear threshold; layer 8 uses a softmax function to output a vector of probabilities by which the input image belongs to individual categories. The numbers of artificial neurons in layer 6 to 8 are 4096, 4096, and 15.

Unlike the original model, we reduced the number of neurons in the output layer from 1000 to 15. The modified categories were indoor, outdoor, people, face, bird, insect, water animal, land animal, flower, fruit, natural scene, car, airplane, ship, exercise. We retrained the last classification layer to have achieved a top-1 test error rate of 14.8%. The retraining images were a subset of ImageNet with ~22,500 training images and 3,000 testing images within the 15 categories. The parameters were optimized using gradient descent with weight decay to minimize the multinomial classification error.

Passing a natural image into the CNN yields an activation value from each artificial neuron; the artificial neurons with a same kernel collectively output a feature map. In this study, we extracted the time-varying feature maps by passing all movie segments frame by frame into the CNN.

Mapping cortical activations with natural movie stimuli. Each segment of the training movie was presented twice to each subject. To find all cortical locations activated by such natural stimuli, for each voxel we computed the cross correlation between the fMRI voxel time series when each subject watched the same movie segment for the first vs. second time. The correlation coefficient was converted to a z score by using the Fisher z-transformation. The voxel-wise z scores were averaged across all 18 segments and tested for significance by using one-sample t-test ($p < 0.01$, DOF=17, Bonferroni correction for the total number of voxels). This average z-map reported the intra-subject reproducibility of fMRI activity during the training movie, reporting the movie-evoked cortical activation. Next, the intra-subject reproducibility maps were averaged across the three subjects in this study. This resulted in an averaged activation map in response to the training movie. From this map, we created a cortical mask to include all significantly activated locations, where the significance was assessed with one-sample t-test on all sessions and all subjects with $p < 0.01$, DOF=17, Bonferroni correction for the total number of voxels. We slightly expanded it for broader applicability to the general population and other natural visual stimuli. The cortical mask contained 10214 voxels in the visual cortex, covering 17.2% of the whole cortical surface.

Preprocessing the CNN outputs. In this study, we compared and related the CNN outputs to cortical fMRI responses, and vice versa. To account for the statistical, timing, and sampling differences between them, we preprocessed the CNN outputs in the following ways. First, all activation time series were logarithmically transformed to match the statistical distribution of the fMRI signals. Second, the log-transformed activation time series were temporally convolved with a canonical hemodynamic response function (HRF) with a positive peak at 4s to account for the hemodynamic delay of the fMRI signal. Lastly, the activation time series was down-sampled to match the timing of fMRI.

Retinotopic mapping. As artificial neurons at the first layer in CNN have well-defined receptive fields and encode local image features, we hypothesize that their activation time series are well aligned with the fMRI signals at early retinotopic visual areas. To test this hypothesis, we computed the cross correlation between the fMRI signal at each cortical location and the activa-

tion time series of every artificial neuron in the first CNN layer in response to the training movie.

For a given cortical location, its cross correlations with the first layer in CNN formed a 3-D array: two dimensions corresponding to the visual field, and the third dimension corresponding to different local image features. This array represented the simultaneous tuning of the fMRI response by retinotopy, orientation, color, and contrast etc. We reduced the 3-D correlation array into a 2-D correlation matrix by taking the maximal correlation across different visual features encoded by the first layer of CNN. The resulting correlation matrix depended only on retinotopy, and reported the population receptive field of the given cortical location. The receptive-field center was determined by calculating the center of the locations with the highest 20 correlation values. The polar angle and the eccentricity of the receptive-field center were quantified for every location on the visual cortex. We compared this retinotopic representation with the visual-field maps obtained with conventional retinotopic mapping, as previously reported in elsewhere (Abdollahi et al., 2014).

Hierarchical mapping. As visual information is processed through multiple cascaded stages in both the CNN and the visual cortex, we hypothesize that different layers in the CNN may be functionally aligned with different regions on the cortex. To test this hypothesis, we computed the cross correlations between the fMRI signal at each cortical location and the activation time series of every artificial neuron at each layer in the CNN. For a given cortical location, we calculated the maximal cross correlation between the fMRI signal and the activation time series from each layer in the CNN. This maximal cross correlation measured the functional alignment between the given cortical location and each CNN layer. Then we identified one layer with the best alignment (i.e. the highest maximal cross-correlation), and assigned its layer index to the given cortical location. The assigned layer index indicated the feed-forward processing stage in which the given cortical location was involved. The cortical distribution of the assigned layer index shows the putative hierarchical mapping of the human visual system.

Mapping fusiform face areas. To explore the functional alignment between the downstream areas and the object categories encoded by layer 8 in the CNN, we examined the cortical fMRI correlates to the “face”-encoding neuron in the CNN. Because the fusiform face area (FFA) is well recognized for face recognition (Johnson, 2005), we hypothesize that the “face” neuron in the CNN is functionally aligned to the FFA. To test this hypothesis, we computed the cross correlation between the activation time series of the “face” neuron and the fMRI signal at every cortical location in re-

sponse to each segment of the training movie. The correlation coefficients were transformed to z scores by Fisher z-transformation, and then averaged across all movie segments. One-sample t-test was used to evaluate the statistical significance of the average cross correlation against zero ($p < 0.01$, $DOF = 17$, Bonferroni correction for the number of voxels).

Encoding: predicting cortical responses to natural visual stimuli. Here, we built voxel-wise encoding models to predict and understand cortical responses to natural visual stimuli. The encoding model included two parts: the first part was used to extract nonlinear stimulus features based on the CNN; the second part was a linear regression model to project the nonlinear feature representations to the fMRI voxel response. For each cortical location, we sought one layer in the CNN where the feature representations could best predict the fMRI response through a linear regression model. In the following, we elaborated the procedures to select and estimate the voxel-wise encoding model.

Given a voxel v , we built a linear regression model to predict the voxel response x based on the l -th layer in the CNN. To simplify the model, we defined the predictors as the outputs from a subset of artificial neurons whose correlations with the given voxel exceeded the half of the maximal correlation within this layer. This model is described as Eq. (1).

$$x_v = \mathbf{Y}^l \mathbf{w}_v^l + \epsilon \quad (1)$$

Here, \mathbf{Y}^l stands for the predictors from the l -th layer. It is an n -by- $(p+1)$ matrix, where n is the number of time points, p is the number of selected artificial neurons; the last column of \mathbf{Y}^l is a constant vector with all elements equal to 1. \mathbf{w}_v^l stands for the regression coefficients. It is a $(p+1)$ -by-1 vector with the last element representing the bias term. ϵ is the error term. For the model estimation, we used the least-squares estimation with L2 regularization. That is, to minimize the cost function in Eq. (2).

$$f(\mathbf{w}_v^l) = \|\mathbf{x}_v - \mathbf{Y}^l \mathbf{w}_v^l\|_2^2 + \lambda_v^l \|\mathbf{w}_v^l\|_2^2 \quad (2)$$

Here, the first term is the sum of squared errors, and the second term is the L2 regularizer imposed on the unknown elements of \mathbf{w}_v^l except the bias component. The regularization parameter λ and the layer index l were both optimized through a 3-fold cross-validation. Briefly, the training data were equally split into three subsets: two for the model estimation, one for the model validation. The validation was repeated three times in order for each subset to be used once for validation. The optimal parameters λ and l were determined as those that gave rise to the highest cross-validation accuracy. With the optimal λ and l , we refitted the model

using the entire training samples to finalize the voxel-wise encoding model.

To test the encoding model, we evaluated the prediction accuracy given the testing movie as the stimuli. Here the accuracy was measured as the cross-correlation between the measured and predicted cortical activity. The significance of the cross correlation was assessed by calculating the p-value with the degree of freedom equal to the number of time points minus 2 (DOF=238, $p < 0.001$, Bonferroni correction for the number of voxels). After evaluating the predictability for each subject, we also compared and averaged the results across subjects.

Deconvolutional neural network (De-CNN). In addition to the CNN, we also used the De-CNN to project any feature representation onto the pixel space. As described in details elsewhere (Zeiler and Fergus, 2014), the De-CNN reverses the operations done by CNN. Specifically, the activations of one or multiple neurons are successively unpooled, rectified, and filtered onto its lower layer, until reaching the input image space. The unpooling step is optional, only applicable to the layers that implement max-pooling. Rectification is conducted as point-wise rectified linear threshold at 0. The filtering step is done by applying the transposed version of the kernels in the CNN to the rectified activations from the immediate higher layer. Neither rectification nor filtering is conditional upon the visual input, whereas the unpooling step is conditional upon the input image. When a visual input is given, we can visualize the internal feature presentation of any neuron of interest by following the deconvolution procedure starting from the selected neuron, while setting the outputs of all other neurons to zeros. In this study, we implemented the De-CNN using the Caffe Deep Learning framework (Jia et al., 2014).

Encoding: visualizing cortical representations at individual voxels. Using the De-CNN as a top-down computational pathway, we visualized the functional representation of a single-voxel response according to the voxel’s encoding model. For a given cortical location, the regression coefficients in its encoding model were used as the exponents, to the power of which the outputs of corresponding artificial neurons were raised, yielding an exponentially weighted distribution of non-linear features. Using the De-CNN, such a weighted feature distribution was projected back to image pixels, giving rise to the visualization of the voxel response. Here, the exponential weighting was used to approximately reverse the linear combination of log-transformed feature representations implemented through the voxel-specific encoding model.

We further extended the visualization to visualize the general functional representation, unbiased by any par-

ticular input, for any given cortical location. For this purpose, we uniformly and randomly sampled 20,400 images of 17 categories (face, cat, insect, indoor furniture, device, bird, outdoor, food, artifact, plant, car, building, fungus, dog, natural scene, airplane, water-animal) from ImageNet. All these images were different from the dataset that we used to train and test the CNN, and they were also different from any frame in the movies that we used to train or test the encoding models. To explore this visualization technique, we selected a voxel at the FFA, and predicted the voxel response to each of the sampled images. The resulting responses were visualized individually, excluding the negative responses, and then averaged to yield a general visualization for the function at the selected voxel. We checked the top 1000 images with the highest predicted voxel responses. Among them, we calculated the percentage of human faces and assessed the significance by using a binomial test against the null hypothesis that the top 1,000 images were uniformly random.

Decoding: reconstruct natural movie stimuli. With the training movie, we estimated multivariate regression models to predict time-varying feature maps of the 1st CNN layer based on distributed cortical fMRI signals. Separate models were trained to estimate the feature maps extracted with different kernels encoded in the 1st layer. For each kernel, a linear model was defined to link the distributed fMRI signals to the output time series of artificial neurons in the CNN, expressed as Eq. (3).

$$\mathbf{Y} = \mathbf{X}\mathbf{W} + \boldsymbol{\epsilon} \quad (3)$$

Here, \mathbf{X} stands for the observed fMRI signals within the visual cortex. It is an n -by- $(m+1)$ matrix, where n is the number of time points, m is the number of voxels; the last column of \mathbf{X} is a constant vector with all elements equal to 1. \mathbf{Y} stands for time-varying feature maps. It was an n -by- p matrix, where n is the number of time points, and p is the number of artificial neurons that encode the given kernel. \mathbf{W} is the unknown weighting matrix in the model. It is an $(m+1)$ -by- p matrix with the last row representing the bias component. $\boldsymbol{\epsilon}$ is the error term.

To estimate the model, we set out to optimize \mathbf{W} to minimize the objective function, as Eq. (4).

$$f(\mathbf{W}) = \|\mathbf{Y} - \mathbf{X}\mathbf{W}\|_2^2 + \lambda \|\mathbf{W}\|_1 \quad (4)$$

Here, the first term is the sum of squares of the estimation errors; the second term represents L1 regularizer imposed on the unknown elements of \mathbf{W} except the bias component; λ is the hyperparameter balancing these two terms.

The model estimation was based on the data collected with the training movie. λ was determined by 20-fold

cross-validation, similar to the procedures used for training the encoding models. For training, we used stochastic gradient descent optimization with the batch size of 100 samples, i.e. only 100 fMRI volumes were utilized in each iteration of training. To address overfitting problem, dropout technique was used by randomly dropping 30% of voxels in every iteration, i.e. setting the dropped voxels to zeros. After we estimated the model for every kernel encoded in the first layer of CNN, the model was directly applied to the fMRI responses to the testing movie to predict the feature maps of every testing-movie frame, according to Eq. (3) without the error term. The predicted feature maps were further exponentially transformed to reverse the logarithmic transformation.

To initially evaluate the performance of the trained decoding models, we conducted 20-fold cross-validation within the training data. The estimation accuracy of the feature map with each kernel was quantified as the cross correlation between the feature maps extracted from CNN and the feature maps estimated from the fMRI signals. The validation accuracy of a kernel was then calculated by averaging the accuracy across repeated validations. Those kernels with low cross-validation accuracy ($r < 0.24$) were excluded in subsequent analyses. 45 kernels were kept for decoding. Those excluded kernels encoded the ‘noisy’ features and color features.

For the 45 kernels selected from cross-validation, we predicted the feature maps of the testing movie based on cortical fMRI responses. For each kernel, the prediction accuracy was quantified as the cross correlation between the fMRI-predicted feature map and that extracted by CNN. The prediction accuracy was averaged across the 45 kernels. To test the statistical significance of the average prediction accuracy, we performed a permutation test. From the fMRI-estimated feature maps, a large set of permuted feature maps were created by randomly and temporally shuffling the estimated feature maps for 10000 times. The cross correlations between the permuted feature maps and the true feature maps were calculated and transformed to z scores by using the Fisher’s r-to-z transformation. This gave rise to a permutation distribution, against which the z-transformed prediction accuracy was compared for significance ($p < 0.01$).

To reconstruct the testing movie frame by frame, the estimated feature maps were deconvolved from the feature space to the pixel space. In the deconvolution step, the transposed version of a kernel in the first layer was used to convolute its corresponding feature map, resulting a deconvolved image. Such deconvolved images from all kernels were then summed up to generate the reconstructed movie frame. Note that such deconvolu-

tion procedure starting from layer 1 to image pixel space only involved in rectification and filtering steps (without unpooling), which was not conditional on the visual stimuli. Therefore, such reconstruction yielded an unbiased reconstruction of the unknown visual experiences.

Decoding: semantic categorization. We built and trained a decoding model to categorize each frame of the testing movie based on cortical fMRI responses. The model was a softmax regression model that estimated the probabilities of 15 object categories from the observed fMRI responses as shown in Eq. (5).

$$p_j = \frac{\exp(\mathbf{w}_j \mathbf{x} + b_j)}{\sum_{i=1}^c \exp(\mathbf{w}_i \mathbf{x} + b_i)} \quad (5)$$

Here, \mathbf{x} is a vector of cortical fMRI responses ($\mathbf{x} = [x_1, \dots, x_m]^T$, m is the number of cortical locations). p_j is the probability of the j -th category. \mathbf{w}_j is a vector of weights used to combine cortical fMRI responses towards predicting p_j ; b_j is the corresponding bias term; c is the total number of categories (i.e. $c=15$).

To train this model, we used CNN to categorize every frame of the training movie, yielding a sample of the true probability of each j -th category, denoted as q_j . The decoding model in Eq. (5) was optimized to maximize the mutual information between the probabilities extracted from CNN and the probabilities predicted from fMRI. That is, to minimize the objective function expressed as Eq. (6).

$$J(\mathbf{w}_{1,\dots,c}, b_{1,\dots,c}) = -\sum_{j=1}^c q_j \log \frac{\exp(\mathbf{w}_j \mathbf{x} + b_j)}{\sum_{i=1}^c \exp(\mathbf{w}_i \mathbf{x} + b_i)} + \lambda \sum_{j=1}^c |\mathbf{w}_j| \quad (6)$$

Here, the second term of the objective function was the L1 regularization, and the hyperparameter λ was determined by 20-fold cross-validation.

After we estimated the model with the training data, we applied the model to cortical fMRI responses to the testing movie. This gave rise to the probability of each testing-movie frame belonging to each of the 15 object categories. The top 5 categories with the highest probabilities were identified, and their labels were used as the frame-by-frame semantic descriptions of the reconstructed testing movie, to facilitate its interpretation.

To evaluate the fMRI-based visual categorization, we used top-1 through top-3 prediction accuracy. Specifically, for each given movie frame, we ranked the object categories in a descending order of the predicted probabilities. If the true object category was the top 1 of the ranked categories, it was considered to be top-1 accurate. If the true object category was the top 2 of the ranked categories, it was considered to be top-2 accurate; so on and so forth. The percentage of top-1/top-2/top-3 accurate frames was used to quantify the predic-

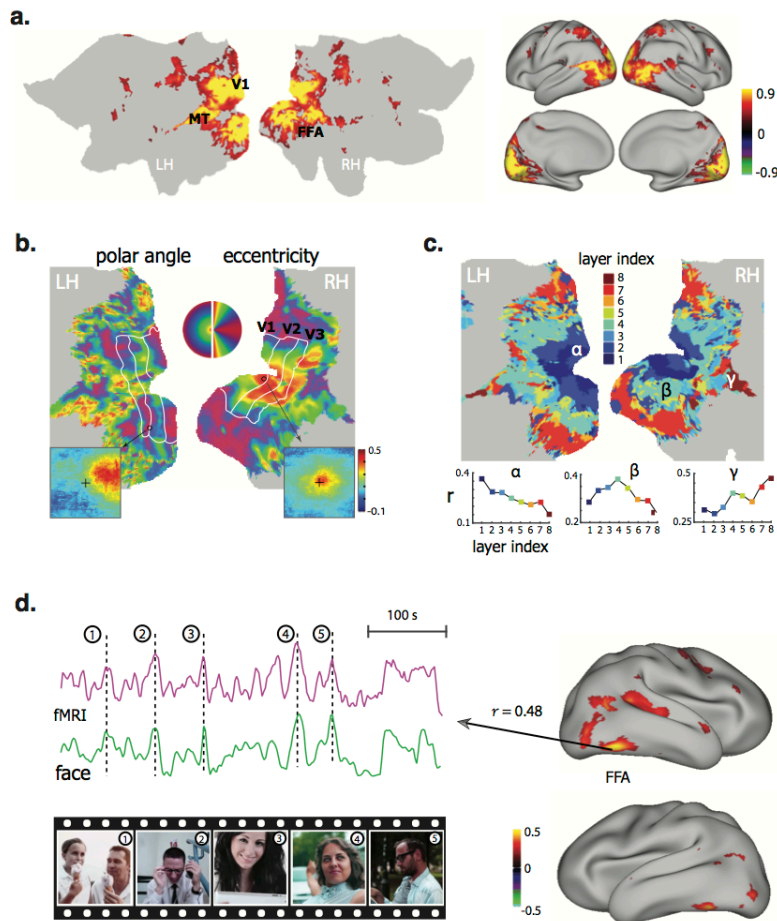


Figure 2. Functional alignment between the visual cortex and the CNN during natural vision (a) **Cortical activation.** The maps show the cross correlations between the fMRI signals obtained during two repetitions of the identical movie stimuli. (b) **Retinotopic mapping.** Cortical representations of the polar angle (left) and eccentricity (right), quantified for the receptive-field center of every cortical location, are shown on the flattened cortical surfaces. The bottom insets show the receptive fields of two example locations from V1 (right) and V3 (left). The V1/V2/V3 borders defined from conventional retinotopic mapping are overlaid for comparison. (c) **Hierarchical mapping.** The map shows the index to the CNN layer most correlated with every cortical location. For three example locations (α , β , γ), their correlations with different CNN layers are displayed in the bottom plots. (d) **Co-activation of FFA and the “Face” neuron.** The maps on the right show the cross correlations between cortical activity and the output time series of the “Face” neuron in the 8th layer of CNN. On the left, the fMRI signal at a single voxel within the FFA is shown in comparison with the activation time series of the “Face” neuron. Movie frames are displayed at five peaks co-occurring in both time series.

tion accuracy. The significance of the prediction accuracy was assessed by one-tail binomial test against the hypothesis that the prediction accuracy was an accuracy of random guesses according to the frequencies of object categories in the training data, while the chance performance was the expected accuracy of random guesses.

Cross-subject encoding & decoding. To demonstrate the feasibility of developing encoders and decoders general to different subjects, we first evaluated the inter-subject reproducibility of the fMRI responses to the same natural movie stimuli across individuals. For each movie segment, we calculated the voxel-wise cross correlation of the fMRI signals between every pair of subjects. The cross-subject reproducibility was obtained by averaging the z-transformed cross correlations across all movie segments. To further obtain the overall reproducibility, we averaged the cross correlation across all pairs of subjects. The statistical significance of the reproducibility against zeros was assessed by using one-sample t-test with the degree of freedom as

the total number of segments minus 1 (DOF=17, Bonferroni correction for the number of voxels, and $p < 0.01$). The cross-subject reproducible cortical locations were very consistent with the defined visual cortex, occupying 82% of the locations within visual cortex ($p < 0.01$, t-test, Bonferroni correction).

For cross-subject encoding, we evaluated the inter-subject predictability of the fMRI responses to a novel natural movie stimulus across individuals. Specifically, we used the encoding models optimized for one subject to predict the cortical fMRI responses for other subjects respectively, and summarized individual cross-subject predictability maps. The prediction accuracy was quantified as the cross correlation between predicted fMRI response and the measured fMRI response. The significance of the cross correlation was assessed by calculating the p-value with the degree of freedom equal to the number of time points minus 2 (DOF=238 with Bonferroni correction to account for the number of voxels and $p < 0.001$). Then we averaged all the individual maps to produce a general cross-subject predictability map.

For cross-subject decoding, we used the decoders trained from one subject’s data to decode another subject’s fMRI data for reconstructing and categorizing the testing movie. The performance of cross-decoding was evaluated in the same way as for within-subject decoding (i.e. training and testing a decoder with data from the same subject).

at every activated cortical location and the output time series of every artificial neuron in the CNN. Since neurons in the first CNN layer received inputs from image patches with a fixed size but at a variable location, their correlations with a given cortical voxel revealed the population receptive field of that voxel (see two examples in the bottom insets in Fig. 2.b). We further charac-

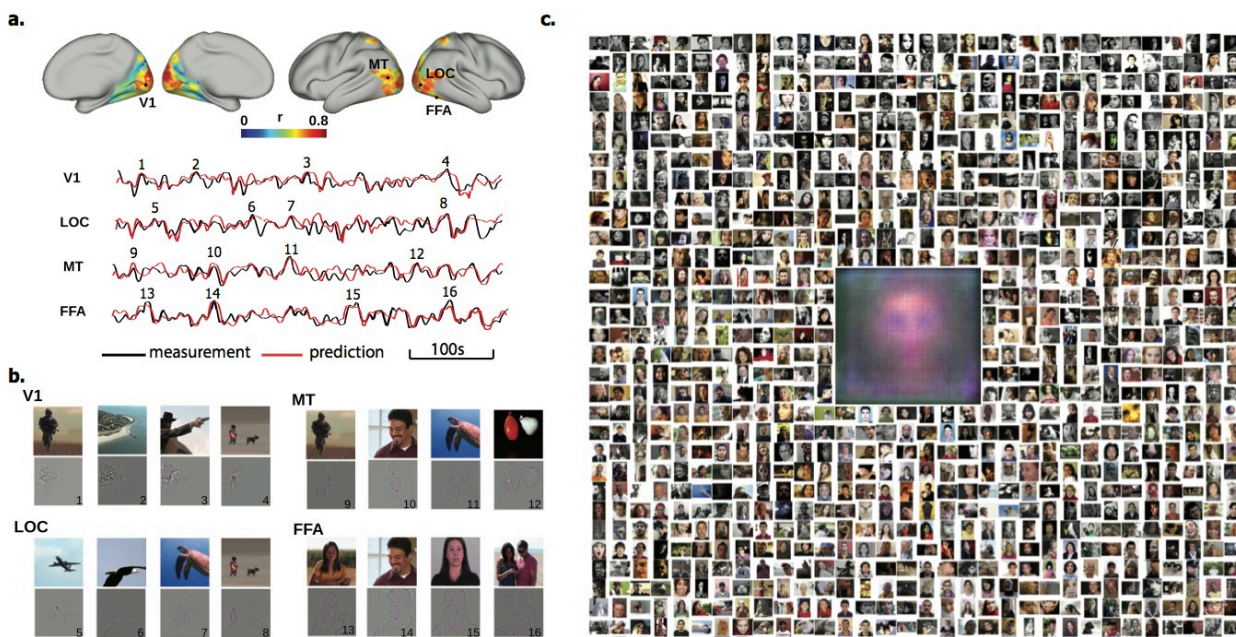


Figure 3. Neural encoding models predict cortical responses and visualize functional representations at individual cortical locations. (a) Cortical predictability for a single subject. Color bar shows the prediction accuracy, i.e. the cross correlation between the measured and predicted responses during the testing movie. The measured (black) and predicted (red) response time series are also shown in comparison for four locations at V1, LOC, MT, and FFA. (b) Visualizations of the four (numbered) peak responses at each of the four locations shown in (a). The presented movie frames are shown in the top; the corresponding visualizations are shown in the bottom. (c) The top 1000 (out of 20,400) pictures that predicted the greatest responses at the FFA voxel are shown in the descending order of the predicted responses.

Results

Functional alignment between CNN and visual cortex

In the training phase, we passed the training movie through the CNN to extract hierarchical features from every movie frame. The output of every artificial neuron in the CNN constituted multiple levels of feature maps, representing increasingly complex and abstract visual information. We asked whether individual cortical locations were selectively aligned to different sets of artificial neurons in the CNN. To address this question, we first mapped the cortical activation with natural vision by evaluating the intra-subject reproducibility of fMRI activity when the subjects watched the training movie for the first vs. second time (Fig. 2.a). The resulting cortical activation was widespread, covering the entire visual cortex and consistent across subjects. We computed the cross correlation between the fMRI signal

terized the receptive field in terms of the polar angle and eccentricity for every cortical voxel, and mapped the retinotopic representation (Fig. 2.b). This map obtained with natural vision shows a similar cortical pattern as the visual-field maps obtained with conventional retinotopic mapping (Wandell et al., 2007). It suggests that every cortical location in early visual areas is functionally aligned to a distinct subset of artificial neurons in the first CNN layer that collectively respond to visual inputs from the receptive field of that location.

Beyond early visual areas, different cortical regions were found to be selectively correlated with distinct layers in the CNN (Fig. 2.c). The lower to higher-level features encoded by the 1st through 8th layers were gradually mapped onto areas from the striate to extrastriate cortex along both ventral and dorsal streams (Fig. 2.c). In agreement with previous findings (Yamins et al., 2014; Güçlü and van Gerven, 2015a,b), this result

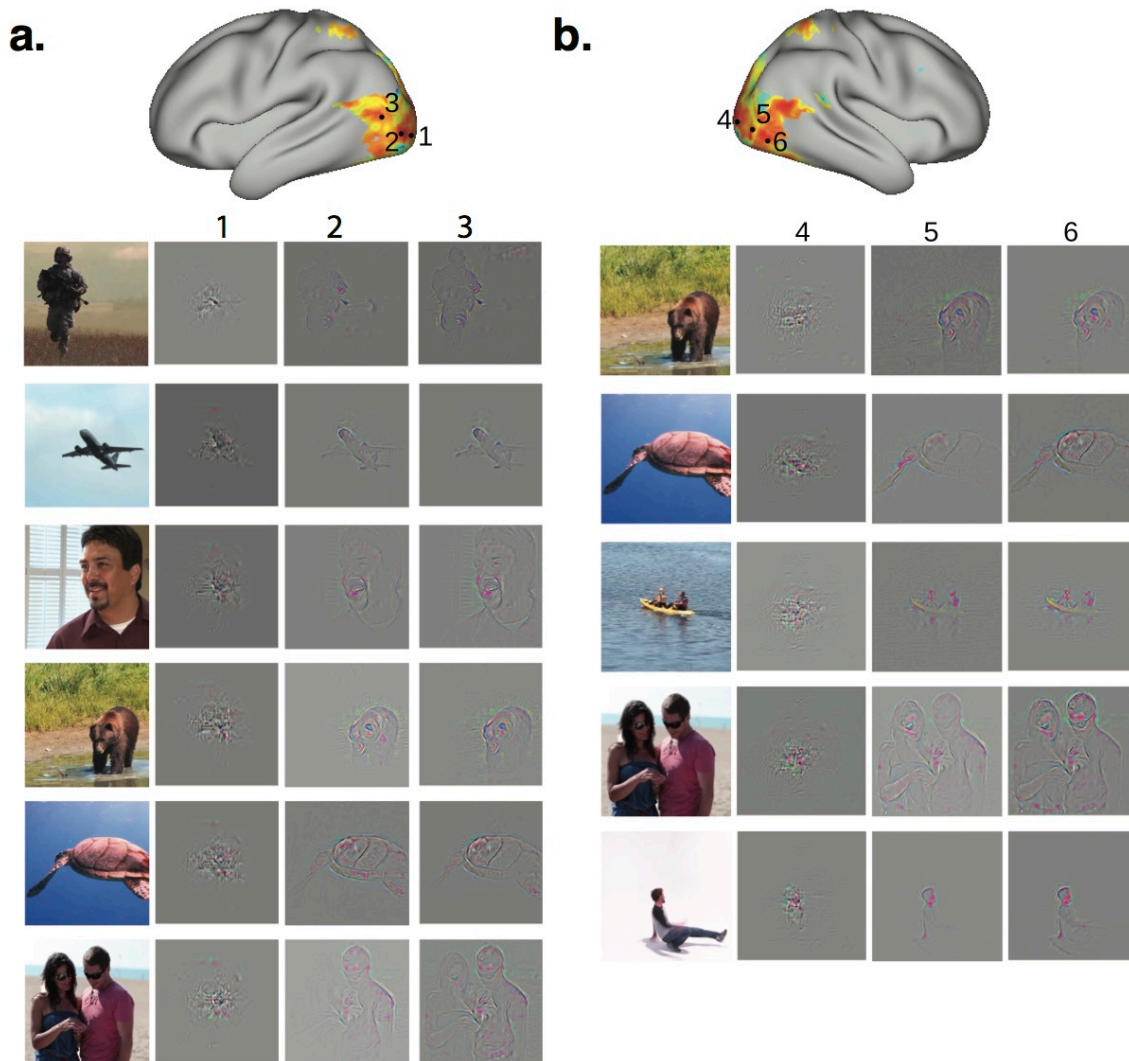


Figure 4. Visualization of the hierarchical visual processing. For six cortical locations from the left and right hemispheres, the visualizations of their responses to multiple movie frames are displayed for comparison.

supports the claim that the brain and the CNN use similar hierarchical representations of visual information. Furthermore, an investigation of the categorical features coded in the CNN revealed a close relationship with the known properties of some visual areas. For example, a ‘face’ neuron in the CNN was significantly correlated with the fusiform face area (FFA) ($r=0.25\pm 0.057$, $p<0.01$, corrected) (Fig. 2.d, right). The fMRI response at the FFA and the output time series of the ‘face’ neuron both showed notable peaks coinciding with movie frames that included human faces (Fig. 2.d, left). Together, these results strongly suggest that the hierarchical layers in the CNN were functionally aligned with cascaded cortical areas along the brain’s visual pathway, including those higher-order areas with semantically specific and perceptually invariant representations.

Neural encoding

Given the functional alignment between the brain and the CNN as demonstrated above, we continued to build and train neural encoding models to predict cortical fMRI responses based on the outputs of the artificial neurons in the CNN. For each cortical location, we selected neurons from a single CNN layer that were most correlated with that location, and combined the log-transformed outputs of the selected neurons to predict the fMRI signal through linear regression. After selecting and estimating the encoding models with the training movie, we tested the prediction accuracy with the testing movie (not included for training the models). As shown in Fig. 3.a, the encoding models could be used to predict the cortical responses to the novel testing movie with high accuracies for nearly the entire visual cortex ($r=0.51\pm 0.09$). Taking as examples four voxels from

the primary visual cortex (V1), lateral occipital complex (LOC), middle temporal (MT), and FFA, their individual responses were best predicted from the outputs of artificial neurons in layer 1, 4, 5, and 7 in the CNN, respectively (Fig. 3.a), suggesting their involvement in progressively later stages of feed-forward visual processing.

Based on its ability to predict cortical responses, the voxel-wise encoding models allowed us to retrieve the visual representations at individual voxels given any natural visual stimulus. That is, to map a single-voxel response in the pixel space to visualize the specific visual-input pattern that causes the response. Briefly, we represented the voxel response as an exponentially weighted distribution of nonlinear features in the CNN (as modeled by the encoding model), and then converted the weighted feature representations back to image pixels by using a top-down projection with the De-CNN. Again, taking the four voxels in V1, LOC, MT, and FFA as examples, we visualized their peak responses given the testing movie to gain intuition about their distinct functions. As shown in Fig. 3.b, the visual representations of the V1 voxel were all confined to a fixed part of the visual field, and showed pixel patterns with local details but lack of any object-defining feature (e.g. shapes). In contrast, the visualizations for the LOC voxel covered a much broader field and delineated some key features indicative of object identity. The MT voxel showed peak responses when the presented movie frames included or implied motion or action; the visualizations of these responses covered the entire visual field, and highlighted the moving parts as opposed to the static surroundings. The FFA voxel showed peak responses only when human faces were presented, and the visualizations were most prominent on face features. In a similar format, we visualized how the same visual inputs were differently represented by six separate cortical voxels from low-, mid-, and high-order areas. Results showed that visual representations were progressively larger and more complex at cortical locations running downstream along the visual pathway (Fig. 4).

While the above visualizations were all conditional upon the testing movie used in our experiments, we further generalized this visualization technique to a much larger set of natural pictures, including 20,400 images randomly and uniformly sampled from 17 categories in ImageNet (Deng et al., 2009; Russakovsky et al., 2015). With this large sample set, we attempt to visualize and understand the general representation at the single-voxel level. As a proof of concept, we focused on the voxel in FFA. The top 1000 pictures that predicted the greatest responses at this voxel were dominantly (90.4%, $p < 10^{-5}$) human faces (Fig. 3.c), while the top 370 pictures were all human faces. To visualize

the general representation of this voxel, we averaged the visualized representations across all 20,400 pictures, regardless of faces or not. Strikingly, the average visualization showed a blurred but discernable picture of a human face (Fig. 3.c, middle). For the first time, this result provides the direct visualization of the highly face-selective functional representation at FFA.

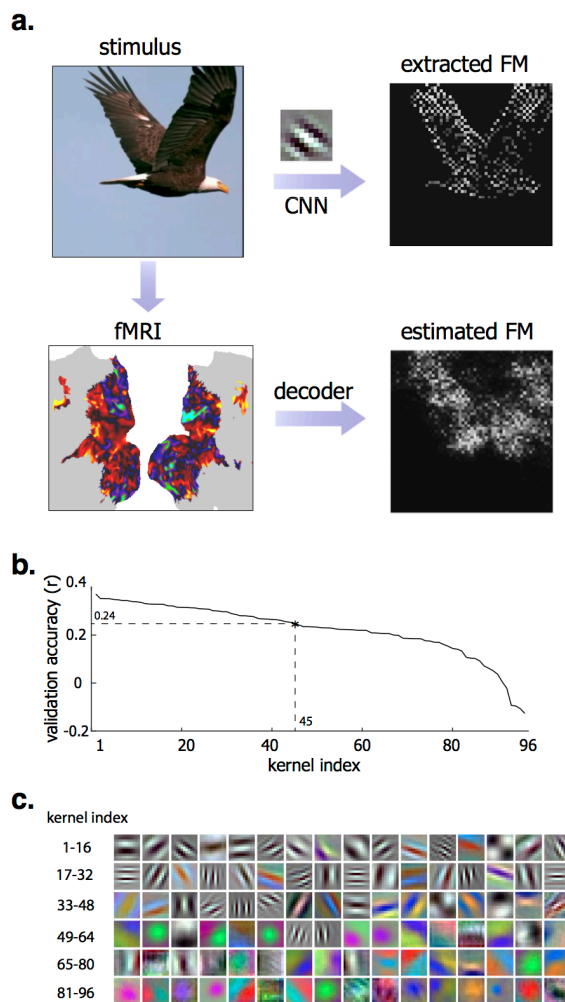


Figure 5. fMRI-based estimation of the first-layer feature maps (FM). (a) For each movie frame, the feature maps extracted from the kernels in the first CNN layer were estimated from cortical fMRI data through decoders trained with the training movie. For an example movie frame (flying eagle) in the testing movie, its feature map extracted with an orientation-coded kernel revealed the image edges. In comparison, the feature map estimated from fMRI was similar, but blurrier. (b) The estimation accuracy for all 96 kernels, given cross-validation within the training data. The accuracies were ranked and plotted from the highest to lowest. Those kernels with high accuracies ($r > 0.24$) were selected and used for reconstructing novel natural movies in the testing phase. (c) 96 kernels in the first layer are ordered in a descending manner according to their cross-validation accuracy.



Figure 6. Reconstruction of a dynamic visual experience. For each row, the top shows the example movie frames seen by one subject; the bottom shows the reconstruction of those frames based on the subject's cortical fMRI responses to the movie. See Movie 1 for the reconstructed movie.

Neural decoding

While the encoding models serve to describe the functional representations of single voxels, the visual and semantic experiences result from distributed patterns of cortical activity that combine various visual features. To account for the distributed neural coding, we seek to build decoding models that combine individual voxel responses in a way to reconstruct visual and semantic experiences. Unlike previous decoding studies (Haxby et al., 2001; Carlson et al., 2002; Thirion et al., 2006; Kay et al., 2008; Nishimoto et al., 2011), our strategy was to establish a computational path to directly transform cortical activity patterns into the visual input and its semantic category in a frame by frame basis. To reconstruct the movie stimuli, we trained a set of multivariate regression models to optimally combine fMRI

signals across cortical voxels in order to estimate every feature map in the first CNN layer. By 20-fold cross-validation within the training data, we could reliably estimate the feature maps of 45 out of 96 features that encoded orientations and edges, but the estimation was less reliable for most color features (Fig. 5). In the testing phase, the trained models were used to convert distributed cortical responses generated by the testing movie to the 45 1st-layer feature maps. The predicted feature maps were similar to the actual feature maps extracted by the CNN ($r=0.30\pm 0.04$). By using the DeCNN, every predicted feature map was further transformed back to the pixel space, where they were combined to reconstruct each frame of the testing movie. Fig. 6 shows sample movie frames reconstructed from fMRI vs. the actual frames presented to the subjects.

The reconstruction clearly captured the location, shape, and movement of salient objects, despite missing color. Note that perceptually less salient objects and the background were poorly reproduced in the reconstructed images. The predominance of foreground elements is likely attributed to their importance in the representation of visual information as measured by fMRI. Thus, the decoding process does not simply reconstruct the original image, but tends to regenerate those image parts that are relevant to visual perception.

To identify object categories from fMRI activity, we defined and optimized a softmax regression model to estimate the vector of normalized probabilities by which each movie frame belonged to 15 categories described with textual labels. In the testing phase, the cortical fMRI activity generated by the testing movie was mapped onto the CNN’s output that predicted categori-

zation probabilities. For selected examples of movie frames, Fig. 7 shows the top five decoded categories, ordered by their probabilities, in comparison with the true categories shown in red. On average, the top-1 and top-3 accuracies were about 49% and 72%, significantly better than chance levels (6.9% and 22.3%) (Table 1). As every category was textually labeled, the decoded categorical information provided frame-by-frame semantic descriptions for the reconstructed movie to facilitate its interpretation. As an example, a flying bird shown in the movie was reconstructed as a bird-like image that was further specifically described as a word “bird” (see the first frame in Fig. 6 & 7). These results suggest that cortical fMRI activity contains rich categorical representations that can be reliably decoded to reconstruct semantic experiences.

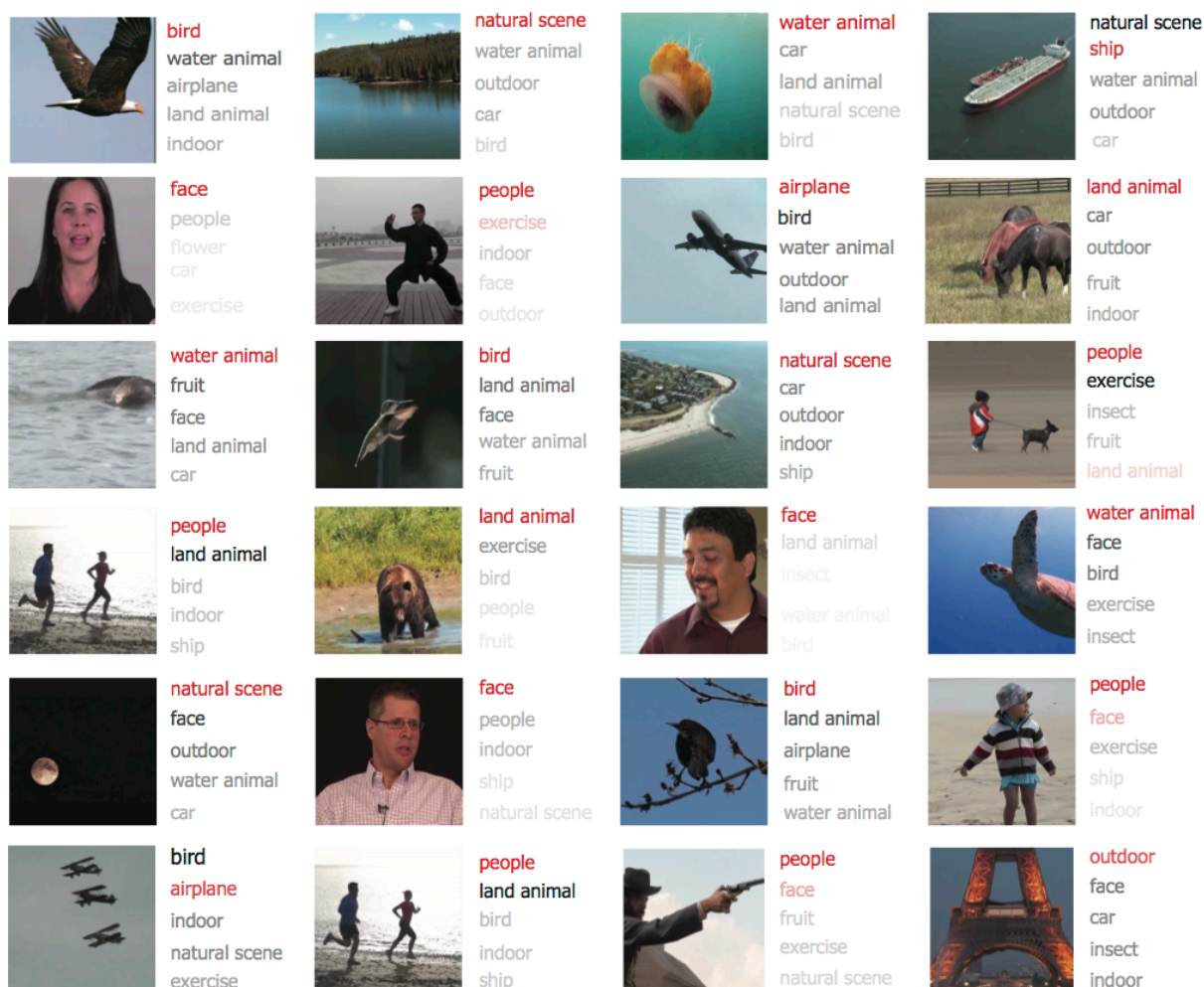


Figure 7. Semantic categorization of natural movie stimuli. For each movie frame, the top five categories determined from cortical fMRI activity are shown in the order of descending probabilities from the top to the bottom. The probability is also color coded in the gray scale with the darker gray indicative of higher probability. For comparison, the true category is shown in red. See Movie 1 for the semantic categorization.

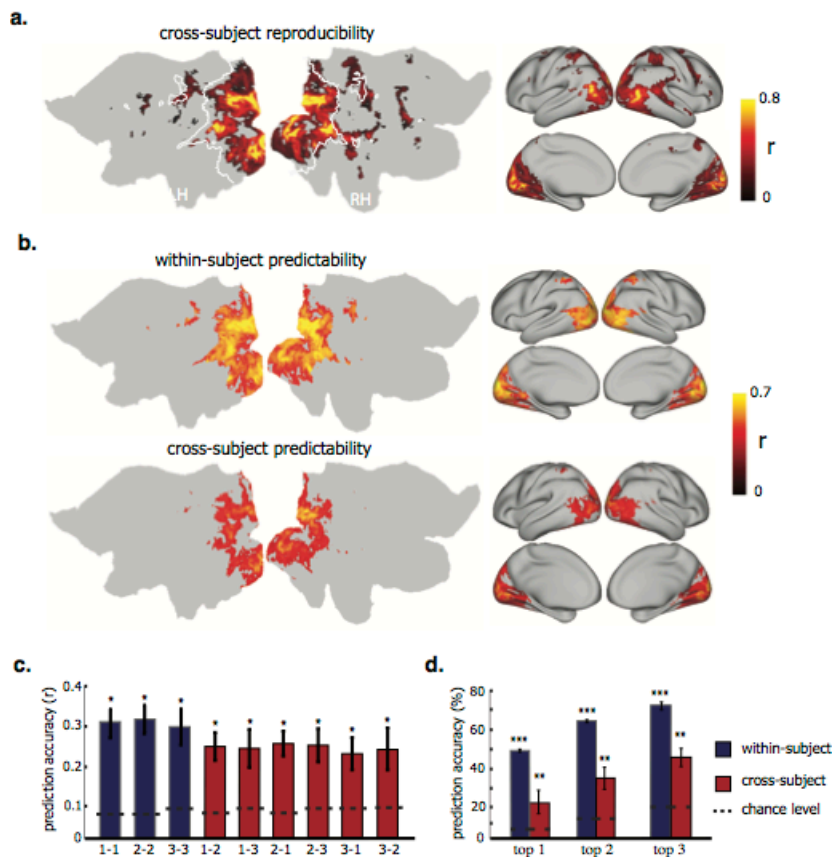


Figure 8. Encoding and decoding within vs. across subjects. (a) Average inter-subject reproducibility of fMRI activity during natural stimuli. (b) Cortical response predictability with encoding models trained and tested for the same subject (i.e. within-subject encoding) or for different subjects (i.e. cross-subject encoding). (c) Accuracy of visual reconstruction by within-subject (blue) vs. cross-subject (red) decoding. The y axis indicates the spatial cross correlation between the fMRI-predicted and CNN-extracted feature maps for the 1st layer in the CNN. The x axis shows multiple pairs of subjects (numbered 1, 2, and 3). The first number indicates the subject from whom the decoder was trained; the second number indicates the subject for whom the decoder was tested. (d) Accuracy of categorization by within-subject (blue) vs. cross-subject (red) decoding. The top-1, top-2 and top-3 accuracy indicates the percentage by which the true category is within the 1st, 2nd, and 3rd most probable categories predicted from fMRI, respectively. For both (c) and (d), the bar height indicates the average prediction accuracy; the error bar indicates the standard error of the mean; the dashed lines are chance levels. (* $p < 10^{-4}$, ** $p < 10^{-10}$, *** $p < 10^{-50}$). See Movie 2 for the reconstructed movie on the basis of cross-subject decoding.

Cross-subject encoding and decoding

Finally, we asked whether it would be feasible to predict and interpret one subject's fMRI activity with the encoding and decoding models trained by data from another subject. In support of this feasibility, we found that different subjects showed similar cortical responses to the same movie (Fig. 8.a), in line with previous findings (Hasson et al., 2004). Encouragingly, the encoding models trained with one subject could predict cortical fMRI responses from another subject with significant, yet reduced, prediction accuracies for most of the visual cortex (Fig. 8.b). For decoding, we found that features in the visual space could be estimated by cross-subject decoding, with reasonable accuracies only slightly lower than when training and testing a decoder within the same subject (Fig. 8.c). In the semantic space, the top-1 through top-3 accuracies for the predicted categories were 22.8%, 35.6% and 46.3% for cross-subject decoding, significantly higher than the chance levels (6.9%, 14.4% and 22.3%), but notably lower than those for within-subject decoding (49.0%, 64.3%, 71.5%) (Fig. 8.d and Table 1). Together, these results provided compelling evidence for the feasibility of establishing neural encoding and decoding models for a general population, while also setting up the baseline for potentially examining the disrupted coding mechanism in pathological conditions.

Prediction accuracy for the semantic descriptions of a novel movie

	train \ test	subject 1	subject 2	subject 3
top 1	subject 1	49.2%	28.8%	13.8%
	subject 2	21.7%	49.6%	23.8%
	subject 3	28.8%	19.6%	48.3%
top 2	subject 1	63.8%	39.2%	27.5%
	subject 2	31.7%	64.6%	36.3%
	subject 3	40.8%	37.9%	64.6%
top 3	subject 1	69.2%	49.2%	41.3%
	subject 2	42.1%	72.9%	46.7%
	subject 3	50.8%	47.5%	72.5%

Table 1. Three subtables show the top-1, top-2 and top-3 accuracies of categorizing individual movie frames by using decoders trained with data from the same (within-subject) or different (cross-subject) subject. Each row shows the prediction accuracy with the decoder trained with a specific subject's training data; each column shows the predicting accuracy with a specific subject's testing data and different subjects' decoders. The accuracy was quantified as the percentage by which individual movie frames were successfully categorized as one of the top-1, top-2, or top-3 categories.

Discussion

This study brings major advances in both neural encoding and decoding for understanding the basis of natural vision. For encoding, we demonstrate the unique promise of using deep learning to model and visualize the functional representations at the single-voxel level along the entire visual pathway, and to create a computational workbench for high-throughput visual neuroscience research. For decoding, we present a stand-alone, efficient, reliable, and generalizable strategy to decode cortical fMRI activity to reconstruct the visual and semantic experiences during natural vision.

The human brain segregates and integrates visual input through cascaded stages of processing. The neural code that describes the relationship between the visual input and the neural response bears a large variety of nonlinearity and complexity (Huth et al., 2016; Yamins and DiCarlo, 2016). It is thus impossible to hand-engineer a general class of models to describe the neural code for every neuron or cortical location, especially for those involved in the middle- or high-level visual processing. In contrast, the CNN entails a large set of nonlinear feature models, as coded by individual artificial neurons through network computation. These feature models provide a family of basis functions, which can be used to define various complex and nonlinear encoding models. Note that each encoding model was separately optimized for each voxel, by specifically selecting an optimal subset of nonlinear features to best match the voxel response with a linear projection. Results suggest that the neural predictability attained with the CNN-based encoding models cover nearly the entire visual cortex, whereas those based on Gabor filters (Daugman, 1985) can only predict responses within the primary visual cortex (Kay et al., 2008). Although our encoding models were used to predict cortical fMRI responses in this study, similar encoding methods would also explain other neural data, such as electrophysiological activity (Yamins et al., 2014). As such, it is expected to offer a general strategy to uncover the complex neural code in various spatial and temporal scales for all levels of visual processing.

It is worth noting that nonlinear features coded in the CNN were not isolated functions, but connected through hierarchical networks that are fully computable either bottom-up or top-down. Thus, a CNN-based encoding model is not only able to predict the response at any given cortical location, but also provides a computational pathway that links the visual input to the localized response, and vice versa. This brings an important advantage in that it allows us to visualize the functional representation at the level of single voxels. Leveraging this advantage, we visualized the progressively larger and more complex representations along the visual

pathway (Fig. 4), showed evidence for distinct functions of multiple cortical areas (Fig. 3.b), and demonstrated the highly selective responses of FFA to human faces (Fig. 3.c). This ability of visualizing the localized functional representation is anticipated to be even more valuable for understanding the responses of single neurons or neuronal ensembles. It would offer a putative computational network basis, in place of the biological circuitry, to account for single-unit or multi-unit activity, despite the usually localized nature of neuronal recordings.

Importantly, we show that the CNN-based encoding models established with natural movie stimuli can be generalized to novel visual stimuli. With this generalizability, one may use the encoding models to predict and analyze cortical responses to a massive amount of natural pictures or videos, much beyond what is practically doable with experimental approaches. In this sense, the encoding models constitute a powerful computational workbench for high-throughput visual neuroscience research. As a proof of concept, here we predicted and characterized the cortical responses to 20,400 natural pictures throughout the entire visual pathway. An in-depth analysis of the responses within FFA revealed its functional selectivity and general representation. Results provide convincing evidence that FFA is exclusively specialized for face perception and its general representation is visualized, for the first time as a human face (Fig. 3.c). Other than FFA, the same computational platform (or its variations) is readily usable to explore cortical representations of other object categories, or to yield novel hypotheses for further experimental investigations.

For the decoding purpose, the CNN enables direct reconstruction of natural movies without using any statistical comparison of activity patterns generated by individual pictures (e.g. classification), which is the common basis of all existing decoding methods, e.g. multivariate pattern analysis (Kamitani and Tong, 2005; Haynes and Rees, 2006; Norman et al., 2006; Miyawaki et al., 2008) and encoding-model-based decoding (Haxby et al., 2001; Kay et al., 2008; Naselaris et al., 2009). Nishimoto et al. (2011) published the first, and perhaps the only, attempt to reconstruct natural movies by searching a huge prior set of videos for the most likely stimuli that would predict the measured cortical activity (Kay et al., 2008). However, this approach is unlikely to scale up because natural visual experiences are too diverse to be fully included in any prior set. The identification or reconstruction accuracy is dependent on and biased by the samples in the prior set. The need for a huge prior set is also computationally expensive, limiting the decoding efficiency.

Bypassing these limitations, we demonstrate that it is possible to directly reconstruct and categorize any natural movie by using a self-contained and well-determined decoder that combine various features across cortical locations. The decoder allowed us to transform fMRI signals onto feature representations at two extreme levels of complexity during early and late visual processing. Through network computation, it also allowed us to transform the decoded feature representations directly onto the pixel space for reconstruction, and onto the semantic space for categorization. By demonstrating this unprecedented decoding ability, we further emphasize the importance of using deep learning for understanding the brain's sensory systems.

In future studies, it is highly desirable to model the visual system with more biologically plausible deep learning models that incorporate feedback (Stollenga et al., 2014) and recurrent (Donahue et al., 2015) connections. The encoding and decoding performance may also serve to evaluate and refine the deep learning models and algorithms towards truly brain-inspired artificial intelligence. In addition, the general strategy described here will benefit from the data acquisition with much more natural images or videos. The diversity and complexity of visual stimuli are expected to improve the reliability and generalizability of the resulting encoding and decoding models. What would also be desirable is the use of neural imaging or recording with higher resolution and sensitivity. For example, the reconstructed dynamic visual experiences missed visual details in texture and color (Fig. 6), mostly because such information is coded in spatiotemporal activity patterns that are difficult to resolve or distinguish with fMRI at the present resolution.

The deep-learning-enabled brain decoding described here as a means to recreate dynamic visual experience has significant potential for reading and reconstructing other sensory or cognitive experiences as well. Since deep-learning models are already available for speech recognitions (Hinton et al., 2012) and language processing (Collobert and Weston, 2008), decoding of brain measures in response to natural hearing, speech, and language are realistically attainable goals (Huth et al., 2016). Likewise, since we know that sensory images, memories and dreams involve neural substrates that overlap with those for real sensation (Kosslyn et al., 1997 ; Horikawa et al., 2013), it is foreseeable that deep-learning models would also be potentially successful in decoding the internal images of the human mind. In addition, deep-learning-based decoding holds the potential to externalize the internal moving images of the mind created through imagination, memory, and dreaming. As the decoding approach expands to other sensory or cognitive systems, we speculate that the ability to decode the internal world of the human mind

through brain decoding will also enable a new form of communication for patients with brain trauma, or neurodegenerative disease.

Acknowledgements: This work was supported in part by NIH R01MH104402 and Purdue Research Foundation. The authors are thankful to Eugenio Culurciello and Alfredo Canziani for their technical support in CNN, to Gregory Francis and Paula Leverage for insightful discussions and suggestions in the paper, to Jiayue Cao for her assistance in experiments.

References

- Abdollahi RO, Kolster H, Glasser MF, Robinson EC, Coalson TS, Dierker D, Jenkinson M, Van Essen DC, Orban GA (2014) Correspondences between retinotopic areas and myelin maps in human visual cortex. *Neuroimage*, 99, pp.509-524.
- Carlson TA, Schrater P, He S (2002) Patterns of activity in the categorical representations of objects. *J. Cogn. Neurosci*, 15, 704-717.
- Cichy RM, Khosla A, Pantazis D, Torralba A, Oliva A (2016) Deep neural networks predict hierarchical spatio-temporal cortical dynamics of human visual object recognition. *arXiv preprint arXiv:1601.02970*.
- Collobert R, Weston J (2008) A unified architecture for natural language processing: Deep neural networks with multitask learning. *Proceedings of the 25th international conference on Machine learning*, 160-167.
- Daugman JG (1985) Uncertainty relation for resolution in space, spatial frequency, and orientation optimized by two-dimensional visual cortical filters. *JOSA A*, 2, 1160-1169.
- Deng J, Dong W, Socher R, Li LJ, Li K, Fei-Fei L (2009) Imagenet: A large-scale hierarchical image database. In *Computer Vision and Pattern Recognition IEEE Conference*, pp.248-255.
- Dicarlo JJ, Zoccolan D, Rust NC (2012) How does the brain solve visual object recognition? *Neuron*, 73, 415-434.
- Donahue J, Hendricks LA, Guadarrama S, Rohrbach M, Venugopalan S, Saenko K, Darrell (2015) Long-term recurrent convolutional networks for visual recognition and description. In *Proceedings of the IEEE Conference on Computer Vision and Pattern Recognition*, pp. 2625-2634.
- Felleman DJ, Van Essen DC (1991) Distributed hierarchical processing in the primate cerebral cortex. *Cerebral cortex*, 1, 1-47.
- Glasser MF, Sotiropoulos SN, Wilson JA, Coalson TS, Fischl B, Andersson JL, Xu J, Jbabdi S, Webster M, Polimeni JR, Van Essen DC (2013) The minimal preprocessing pipelines for the Human Connectome Project. *Neuroimage*, 80, pp.105-124.
- Güçlü U, van Gerven MA (2015a) Deep neural networks reveal a gradient in the complexity of neural representations across the ventral stream. *The Journal of Neuroscience*, 35, 10005-10014.
- Güçlü U, van Gerven MA (2015b) Increasingly complex representations of natural movies across the dorsal stream are shared between subjects. *NeuroImage*, in press.

- Hasson U, Nir Y, Levy I, Fuhrmann G, Malach R (2004) Inter-subject synchronization of cortical activity during natural vision. *Science*, 303(5664), pp.1634-1640.
- Haxby JV, Gobbini MI, Furey ML, Ishai A, Schouten JL, Pietrini P (2001) Distributed and overlapping representations of faces and objects in ventral temporal cortex. *Science*, 293(5539), pp.2425-2430.
- Haynes JD, Rees G (2006) Decoding mental states from brain activity in humans. *Nature Reviews Neuroscience*, 7, 523-534.
- Hinton G, Deng L, Yu D, Dahl GE, Mohamed AR, Jaitly N, Senior A, Vanhoucke V, Nguyen P, Sainath, TN, Kingsbury B (2012) Deep neural networks for acoustic modeling in speech recognition: The shared views of four research groups. *IEEE Signal Processing Magazine*, 29(6), pp.82-97.
- Horikawa T, Tamaki M, Miyawaki Y, Kamitani Y (2013) Neural decoding of visual imagery during sleep. *Science*, 340, 639-642.
- Huth AG, de Heer WA, Griffiths TL, Theunissen FE, Gallant JL (2016) Natural speech reveals the semantic maps that tile human cerebral cortex. *Nature*, 532(7600), pp.453-458.
- Huth AG, de Heer WA, Griffiths TL, Theunissen FE, Gallant JL (2016) Natural speech reveals the semantic maps that tile human cerebral cortex. *Nature*, 532(7600), pp.453-458.
- Jia Y, Shelhamer E, Donahue J, Karayev S, Long J, Girshick R, Guadarrama S, Darrell T (2014) Caffe: Convolutional architecture for fast feature embedding. In *Proceedings of the 22nd ACM international conference on Multimedia*, pp. 675-678.
- Johnson MH (2005) Subcortical face processing. *Nature Reviews Neuroscience*, 6, 766-774.
- Kamitani Y, Tong F (2005) Decoding the visual and subjective contents of the human brain. *Nature neuroscience*, 8, 679-685.
- Kay KN, Naselaris T, Prenger RJ, Gallant JL (2008) Identifying natural images from human brain activity. *Nature*, 452, 352-355.
- Khaligh-Razavi SM, Kriegeskorte N (2014) Deep supervised, but not unsupervised, models may explain IT cortical representation. *PLoS Comput Biol*, 10(11), e1003915.
- Kosslyn SM, Thompson WL, Alpert NM (1997) Neural systems shared by visual imagery and visual perception: A positron emission tomography study. *Neuroimage*, 6, 320-334.
- Krizhevsky A, Sutskever I, Hinton GE (2012) Imagenet classification with deep convolutional neural networks. *Advances in neural information processing systems*, 1097-1105.
- LeCun Y, Bengio Y, Hinton G (2015) Deep Learning. *Nature*, 521, 436-444.
- Miyawaki Y, Uchida H, Yamashita O, Sato MA, Morito Y, Tanabe HC, Sadato N, Kamitani Y (2008) Visual image reconstruction from human brain activity using a combination of multiscale local image decoders. *Neuron*, 60(5), pp.915-929.
- Naselaris T, Prenger RJ, Kay KN, Oliver M, Gallant JL (2009) Bayesian reconstruction of natural images from human brain activity. *Neuron*, 63(6), pp.902-915.
- Nishimoto S, Vu AT, Naselaris T, Benjamini Y, Yu B, Gallant JL (2011) Reconstructing visual experiences from brain activity evoked by natural movies. *Current Biology*, 21(19), pp.1641-1646.
- Norman KA, Polyn SM, Detre GJ, Haxby JV (2006) Beyond mind-reading: multi-voxel pattern analysis of fMRI data. *Trends in cognitive sciences*, 10, 424-430.
- Russ BE, Leopold DA (2015) Functional MRI mapping of dynamic visual features during natural viewing in the macaque. *NeuroImage*, 109, 84-94.
- Russakovsky O, Deng J, Su H, Krause J, Satheesh S, Ma S, Huang Z, Karpathy A, Khosla A, Bernstein M, Berg AC (2015) Imagenet large scale visual recognition challenge. *International Journal of Computer Vision*, 115(3), pp.211-252.
- Stollenga MF, Masci J, Gomez F, Schmidhuber J (2014) Deep networks with internal selective attention through feedback connections. *Advances in Neural Information Processing Systems*, 3545-3553.
- Thirion B, Duchesnay E, Hubbard E, Dubois J, Poline JB, Lebihan D, Dehaene S (2006) Inverse retinotopy: inferring the visual content of images from brain activation patterns. *Neuroimage*, 33(4), pp.1104-1116.
- Wandell BA, Dumoulin SO, Brewer AA (2007) Visual field maps in human cortex. *Neuron*, 56, 366-383.
- Yamins DL, DiCarlo JJ (2016) Using goal-driven deep learning models to understand sensory cortex. *Nature neuroscience*, 19, 356-365.
- Yamins DL, Hong H, Cadieu CF, Solomon EA, Seibert D, DiCarlo JJ (2014) Performance-optimized hierarchical models predict neural responses in higher visual cortex. *Proceedings of the National Academy of Sciences*, 111(23), pp.8619-8624.
- Zeiler MD, Fergus R (2014) Visualizing and understanding convolutional networks. *European Conference on Computer Vision*, Springer International Publishing, 818-833.